Supporting Information

Water in Carbon Nanotubes: Pronounced Anisotropy in the Dielectric Dispersion and Its Microscopic Origin

Sayantan Mondal and Biman Bagchi*

Solid State and Structural Chemistry Unit
Indian Institute of Science, Bengaluru. India

*corresponding author's email: bbagchi@iisc.ac.in

1. Derivation of the linear response relations Eq. (4) and (5) in the main text

In the following we provide a detailed derivation of equations (5) and (6) of the main text used to obtain the reported numerical results. The derivation closely follows the formalisms described by Fröhlich,[1] Jackson[2] and Zhan[3]. According to the theory of macroscopic dielectrics the two fundamental equations that define the dielectric response of a system are equations (SI.1) and (SI.2).[1-3]

$$\mathbf{D} = \underline{\underline{\boldsymbol{\varepsilon}}}\mathbf{E} \tag{SI.1}$$

$$\mathbf{D} = \mathbf{E} + 4\pi\mathbf{P} \tag{SI.2}$$

Here, **E** is the Maxwell field, **D** is the electric displacement vector, **P** is the polarisation, and $\underline{\underline{\boldsymbol{\varepsilon}}}$ is the dielectric tensor. For an isotropic system all three eigenvalues of $\underline{\underline{\boldsymbol{\varepsilon}}}$ are the same. However, because of the asymmetry of the confining geometry, the eigenvalues might be unequal. If one eliminates **D** from equations (SI.1) and (SI.2), one obtains equation (SI.3).

$$\boldsymbol{\varepsilon} = \mathbf{1} + 4\pi\left(\frac{\mathbf{P}}{\mathbf{E}}\right) \tag{SI.3}$$

The main problem with equation (SI.3) is that the occurrence of two unknowns in one equation, namely, the static dielectric constant and the ratio (**P**/**E**). If one assumes the applied field is weak, the application of Kubo's linear response formalism provides analytical expressions as detailed below.[4]

The total dipole moment (that is proportional to the polarisation) couples with the cavity field ($\mathbf{E}_c$) which modifies the Hamiltonian of the system. The cavity field is

proportional to the external field emerging from infinity but in general not equal. Polarisation (**P**) inside a material is defined as the total dipole moment (**M**) per unit volume (V). However, in dipolar liquids, the excess average polarisation due to the external field determines the dielectric constant. Hence, it is better to formulate the subsequent equations in terms of the polarisation fluctuation $(\Delta\mathbf{P})$ rather than the polarisation (**P**) itself. The fluctuation in the polarisation after the application of the external field can be written as

$$\Delta\mathbf{P} = \frac{1}{V}\left[\mathbf{M} - \langle\mathbf{M}\rangle_0\right], \tag{SI.4}$$

Where, $\langle ... \rangle_0$ denotes ensemble average without the applied field which are observables in macroscopic measurements. The phase space average of equation (SI.4) can be written as

$$\langle\Delta\mathbf{P}\rangle = \frac{1}{V}\frac{\int d\mathbf{r}^N \left(\mathbf{M} - \langle\mathbf{M}\rangle_0\right)\exp\left[-\beta\left\{U(\mathbf{r}^N) - \mathbf{M}.\mathbf{E}_c\right\}\right]}{\int d\mathbf{r}^N \exp\left[-\beta\left\{U(\mathbf{r}^N) - \mathbf{M}.\mathbf{E}_c\right\}\right]}, \tag{SI.5}$$

where, $U(\mathbf{r}^N)$ is the many-body potential energy of the system and $(-\mathbf{M}.\mathbf{E}_c)$ is the additional energy due to the interaction with the cavity field. Below we outline the derivation of the linear response relations by considering weak $\mathbf{E_c}$. First, we separate out the $\exp(\beta\mathbf{M}.\mathbf{E}_c)$ term and expand it up to the first (linear) term.

$$\begin{aligned}\exp\left[-\beta\left\{U(\mathbf{r}^N) - \mathbf{M}.\mathbf{E}_c\right\}\right] &= \exp\left[-\beta U(\mathbf{r}^N)\right]\exp\left(\beta\mathbf{M}.\mathbf{E}_c\right) \\ &\approx \left(1 + \beta\mathbf{M}.\mathbf{E}_c\right)\exp\left[-\beta U(\mathbf{r}^N)\right]\end{aligned} \tag{SI.6}$$

We insert the expression obtained from equation (SI.6) into equation (SI.5) to obtain equation (SI.7).

$$\begin{aligned}\langle\Delta\mathbf{P}\rangle &\approx \frac{1}{V}\left[\frac{1}{Z}\int d\mathbf{r}^N \left(\mathbf{M} - \langle\mathbf{M}\rangle_0\right)\left(1 + \beta\mathbf{M}.\mathbf{E}_c\right)\exp\left\{-\beta U(\mathbf{r}^N)\right\}\right] \\ &= \frac{1}{V}\left[\begin{array}{l}\frac{1}{Z}\int d\mathbf{r}^N \mathbf{M}\exp\left\{-\beta U(\mathbf{r}^N)\right\} - \frac{1}{Z}\int d\mathbf{r}^N \langle\mathbf{M}\rangle_0 \exp\left\{-\beta U(\mathbf{r}^N)\right\} \\ + \frac{1}{Z}\int d\mathbf{r}^N \left(\beta\mathbf{M}^2\mathbf{E}_c\right)\exp\left\{-\beta U(\mathbf{r}^N)\right\} - \frac{1}{Z}\int d\mathbf{r}^N \left(\beta\mathbf{M}\mathbf{E}_c\right)\langle\mathbf{M}\rangle_0 \exp\left\{-\beta U(\mathbf{r}^N)\right\}\end{array}\right]\end{aligned} \tag{SI.7}$$

Where, $Z = \int d\mathbf{r}^N \exp[-\beta U(\mathbf{r}^N)]$. After simplifying equation (SI.7) one obtains

$$\langle \Delta \mathbf{P} \rangle \approx \frac{\beta}{V}[\langle \mathbf{M}^2 \rangle_0 - \langle \mathbf{M} \rangle_0^{\,2}].\mathbf{E}_c \,. \tag{SI.8}$$

Hence, the ratio of polarisation fluctuation to the cavity field can be replaced by $\frac{\beta}{V}[\langle \mathbf{M}^2 \rangle_0 - \langle \mathbf{M} \rangle_0^{\,2}]$ for the weak field approximation where $\beta = (k_B T)^{-1}$. This relation shall be use later in this section.

Now, we aim to obtain the cavity fields inside the cylinder to define effective dielectric constants for externally imposed electric fields from different directions. We depict the situations schematically in **Figure S1.**

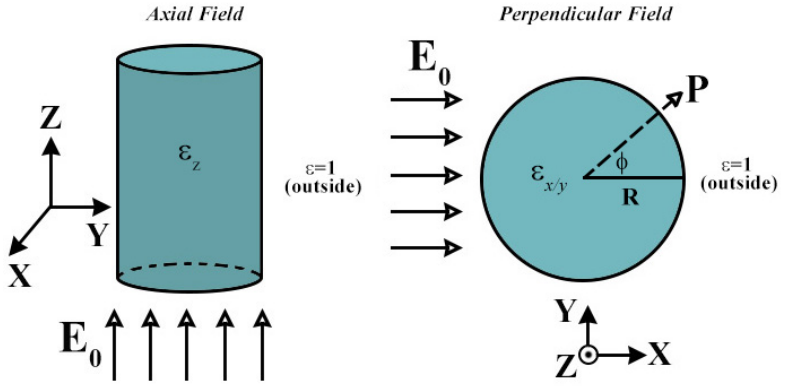

Figure S1. Schematic illustration to show the placement of the cylinder and the external fields in order to probe different components of the anisotropic dielectric tensor. The infinitely long cylinder is aligned along the Z axis and suspended in vacuum ($\varepsilon = 1$). In case of the external field ($\mathbf{E}_0$) along Z, the cavity field becomes equal to $\mathbf{E}_0$ as the two ends are open and no dielectric boundaries are present. This gives us the axial dielectric response. For the perpendicular field (either from X or Y directions in the Cartesian frame), the cavity field gets modified by a factor to be determined from the cylindrical dielectric boundary conditions. This provides the perpendicular (with respect to the CNT axis) dielectric response.

For the axial field, the cavity field is equal to the externally applied field, $\mathbf{E}_c^z = \mathbf{E}_0$. Hence, equation (SI.3) becomes,

$$\varepsilon_z = 1 + 4\pi\left(\frac{\mathbf{P}_z}{\mathbf{E}_c^z}\right) = 1 + 4\pi\left(\frac{\mathbf{P}_z}{\mathbf{E}_0}\right) \tag{SI.9}$$

By applying equation (SI.8) one obtains equation (4) in the main text [here, Eq.(SI.10)] where, $M_z = \mathbf{M}.\hat{\mathbf{e}}_z$.

$$\varepsilon_z = 1 + \frac{4\pi\beta}{V}\left[\langle M_z^2 \rangle_0 - \langle M_z \rangle_0^{\,2}\right] \tag{SI.10}$$

To obtain $\mathbf{E_c}$ for the perpendicular field we follow the procedure described by Markus Zhan.[3] Let us consider a potential function, $\psi(r,\phi)$, that is dependent on the radial (r) and azimuthal coordinate (ϕ) inside a cylinder. We write down the guess solutions for $\psi(r,\phi)$ as obtained from the solution of the Laplace equation.[2-3]

$$\begin{aligned}\psi(r,\phi) &= Ar\cos\phi; \qquad \text{for } r \le R \\ &= \left[Br + \frac{C}{r}\right]\cos\phi; \quad \text{for } r \ge R\end{aligned} \tag{SI.11}$$

The coefficients *A*, *B* and *C* can be determined subject to the following two boundary conditions,

$$-\frac{1}{R}\frac{\partial}{\partial\phi}\psi(r<R,\phi)\Big|_{r=R} = -\frac{1}{R}\frac{\partial}{\partial\phi}\psi(r>R,\phi)\Big|_{r=R} \tag{SI.12}$$

$$\varepsilon_{x/y}\frac{\partial}{\partial r}\psi(r<R,\phi)\Big|_{r=R} = \frac{\partial}{\partial r}\psi(r>R,\phi)\Big|_{r=R}. \tag{SI.13}$$

Now, the electric field inside and outside the cylinder can be evaluated as $-grad\,\psi(r,\phi)$ where the *grad* operator in the cylindrical coordinate is given by $\left[\frac{\partial}{\partial r}\hat{\mathbf{e}}_{\mathbf{r}} + \frac{1}{r}\frac{\partial}{\partial\phi}\hat{\mathbf{e}}_{\phi} + \frac{\partial}{\partial z}\hat{\mathbf{e}}_{\mathbf{z}}\right]$. Here, $\hat{\mathbf{e}}_{\mathrm{r}}, \hat{\mathbf{e}}_{\phi}$ and $\hat{\mathbf{e}}_{z}$ denote the unit vectors. Hence one obtains the electric fields as

$$\begin{aligned}\mathbf{E}(r<R) &= -A\left[\cos\phi\,\hat{\mathbf{e}}_{\mathrm{r}} - \sin\phi\,\hat{\mathbf{e}}_{\phi}\right] = -A\hat{\mathbf{e}}_{\mathbf{x}} = \mathbf{E}_c \\ \mathbf{E}(r>R) &= -\left[B - \frac{C}{r^2}\right]\cos\phi\,\hat{\mathbf{e}}_{\mathrm{r}} + \left[B + \frac{C}{r^2}\right]\sin\phi\,\hat{\mathbf{e}}_{\phi}\end{aligned}. \tag{SI.14}$$

We assume that the externally applied field is emerging from $x \to \infty$ in the Cartesian frame (or, $r \to \infty$ in the cylindrical coordinate frame). Here, another boundary condition must be valid: $\lim_{r\to\infty}\mathbf{E}(r>R) = -E_0\hat{\mathbf{e}}_{\mathbf{x}}$. This is equivalent of writing $B = -\mathbf{E_0}$. By employing the two boundary conditions for the continuity of the tangential and normal fields [Eqs. (SI.12) and (SI.13)] we obtain

$$AR = BR + \frac{C}{R} \tag{SI.15}$$

$$\text{and, } \varepsilon_{x/y} A = B - \frac{C}{R^2}. \tag{SI.16}$$

By solving the above equations we obtain the expressions of *A* and *C* in terms of the external field (**$\mathbf{E_0}$**) and the effective dielectric constant perpendicular to the Z-direction ($\varepsilon_{x/y}$).

$$A = -\left(\frac{2}{\varepsilon_{x/y}+1}\right)\mathbf{E}_0 \text{ and } C = \left(\frac{\varepsilon_{x/y}-1}{\varepsilon_{x/y}+1}\right)R^2\mathbf{E}_0 \tag{SI.17}$$

Hence, according to equation (SI.14) the cavity field $\left(\mathbf{E}_c^{x/y}\right)$ becomes

$$\mathbf{E}_c^{x/y} = -A\hat{\mathbf{e}}_\mathbf{x} = \frac{2}{\varepsilon_{x/y}+1}\mathrm{E}_0\hat{\mathbf{e}}_\mathbf{x}. \tag{SI.18}$$

Finally, we obtain the expression for $\varepsilon_{x/y}$ from equation (SI.3) as

$$2\left(\frac{\varepsilon_{x/y}-1}{\varepsilon_{x/y}+1}\right) = 4\pi\left(\frac{\mathbf{P}_{x/y}}{\mathbf{E}_0}\right). \tag{SI.19}$$

By the application of linear response relation [Eq. (SI.8)] we arrive at the following expression [Eq. (SI.20)] where, $M_{x/y} = \left(\mathbf{M}.\hat{\mathbf{e}}_\mathbf{x} + \mathbf{M}.\hat{\mathbf{e}}_\mathbf{y}\right)$. This is the equation (5) used in the main text.

$$\frac{\varepsilon_{x/y}-1}{\varepsilon_{x/y}+1} = \frac{2\pi\beta}{V}\left[\left\langle M_{x/y}^2\right\rangle_0 - \left\langle M_{x/y}\right\rangle_0^2\right] \tag{SI.20}$$

2. System and simulation details

We have performed classical atomistic molecular dynamics simulations of single walled carbon nanotubes (CNT) suspended in vacuum with their cylindrical cavities filled with SPC/E water. We have modelled six CNT-water systems of fixed length (L=5 nm) but different diameters (d ~ 1.3 nm, 1.6 nm, 2.0 nm, 3.0 nm, 4.0 nm and 5.0 nm) depending on the chiral indices (*m*,*n*) of the CNT. The CNTs have been placed at the centre of the box and aligned with the Z-direction (box length along z is 5.34 nm). Hence, we have employed periodic boundaries in the Z-direction only which makes it an infinitely long CNT along Z. We have inserted the average number of water molecules (N_{wat}) obtained from another set of 10 ns long equilibrium MD trajectories where the cylinder have been immersed inside a

tetragonal box filled with SPC/E water molecules so that a water bath is present. The system details have been provided in **Table S1**.

Table S1. System specifications for the aqueous carbon nanotube simulations.

Chiral Indices (*m*,*n*)	Diameter (nm)	N_{wat}
(10,10)	1.35	120
(12,12)	1.62	198
(15,15)	2.03	340
(22,22)	2.98	870
(30,30)	4.06	1,740
(37,37)	5.01	2,768

Throughout the simulations, the CNT coordinates have been kept frozen. The wall atoms of the CNTs are uncharged. Hence, the altered results reported in the main letter are due to the influence of the geometrical confinement only. We have provided the force field parameters in **Table S2**.

Table S2. The force-field parameters for carbon nano tube (CNT) and SPC/E water used in the present study. The water molecules possess a permanent dipole moment of 2.35 debye whereas the CNT wall atoms are modelled as non-polarisable Lennard-Jones particles.[5-6]

	$\sigma\,(nm)$	$\varepsilon\,(kCal\,mol^{-1})$	q/e	$bond\ length\,(nm)$	*Angle*
Water (SPC/E)	0.316	0.155	q_O=-0.8476, q_H=+0.4238	$d_{O-H}=0.10$	$\theta_{H\hat{O}H}=109.47^{\circ}$
CNT atoms	0.34	0.09	uncharged	$d_{C-C}=0.142$	$\theta_{C\hat{C}C}=120^{\circ}$

We have used leap-frog integrator with 2 fs time step to propagate the systems in NVT ensembles (T=300 K). After energy minimisation by steepest descent algorithm, 10 ns NVT equilibrations have been performed. The lengths of the MD trajectories are 100 ns by which the cumulative mean squared dipole moment fluctuations have been converged. We have recorded the coordinates in each 10 fs to obtain the dielectric relaxation spectrum. Nose-Hoover thermostat ($\tau_T = 0.21\,ps$) has been employed to maintain the temperature of the systems at ~300K. For the simulations with water bath, we have performed an additional 5 ns initial equilibration with Parrinello-Rahman barostat ($\tau_P = 2.0\,ps$ and $P_{ref} = 1bar$) before the NVT equilibration followed by NVT production run.

We have employed Particle-Mesh-Ewald with FFT grid spacing of 0.16 Å to incorporate long-range electrostatics. Coulomb and van Der Waals cut-offs have been chosen to be 12 Å.

For the bulk, we have simulated separately a cubic box of dimensions (5x5x5) nm^3 that contains 4,071 water molecules at 300 K in an NVT ensemble for 10 ns with the same parameters. All the MD simulations have been performed using GROMACS 5.1.4[7] and the analyses have been performed using in-house codes in FORTRAN and MATLAB (*version* 9.4).

We have used the following criteria [Eq.(SI.21)] to obtain the average number of water molecules inside CNTs, from the simulations with water bath.

$$\begin{aligned} r &< R \\ z_l \leq z_{Oxygen} &\leq z_u \end{aligned} \qquad \text{(SI.21)}$$

Here, r is the distance of the oxygen atom of a selected water molecule from the CNT axis, R is the cut-off distance at which the CNT wall ends, Z_l and Z_u are the lower and upper Cartesian z-coordinates of the CNT and Z_{Oxygen} is the z-coordinate of the oxygen atom of the water molecule under consideration. Below, we provide a schematic picture (**Figure S2**).

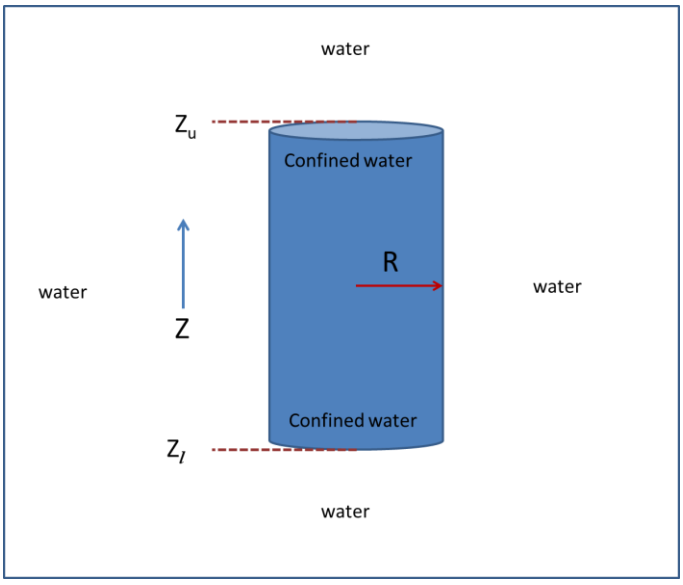

Figure S2. The scheme and cut-off regions to obtain the average number of confined water molecules inside nanocylinders from simulations with CNTs attached to water bath. The average numbers, thus obtained, are used to fix the number density inside the infinite CNTs suspended in vaccum.

3. Sensitivity towards the effective volume and numerical values of static dielectric constants with error estimates

We rearrange equation (SI.20) as

$$\varepsilon_{x/y} = \frac{V + 2\pi\beta\left\langle \delta M_{x/y}^2 \right\rangle}{V - 2\pi\beta\left\langle \delta M_{x/y}^2 \right\rangle}. \tag{SI.22}$$

Hence, $\varepsilon_{x/y}$ diverges if $V = 2\pi\beta\left\langle \delta M_{x/y}^2 \right\rangle$. We find that the value of $\varepsilon_{x/y}$ is quite sensitive towards the estimated effective volume. Because of the nature of the Lennard-Jones interactions and geometrical constraints the accessible volume by the water molecules becomes less than $V = \pi R^2 L$. In the main text we have addressed this issue. Below we describe the numerical procedure followed to obtain the effective radius (r_{eff}) and effective volume (V_{eff}).

In the main text, we show the radial number density profiles (**Figure 2b**). From the density profiles, that is, $\rho(r)$ vs r plots, we obtain the effective diameter by using the following equation [(SI.23)]

$$\frac{1}{N_{wat}} \int_0^{r_{eff}} dr\, r\, (2\pi L)\, \rho(r) = 1 \tag{SI.23}$$

Therefore, we vary the upper limit (r_{eff}) of the integral from 0 to R and choose the lowest value of r_{eff} for which the integral $\int_0^{r_{eff}} dr\, r\, (2\pi L)\, \rho(r)$ yields the total number of confined water molecules (N_{wat}). The obtained values of r_{eff} are used to calculate V_{eff} $\left(= \pi r_{eff}^2 L\right)$. Here, in **Figure S3**, we demostrate the sensitivity of $\varepsilon_{x/y}$ towards the effective volume.

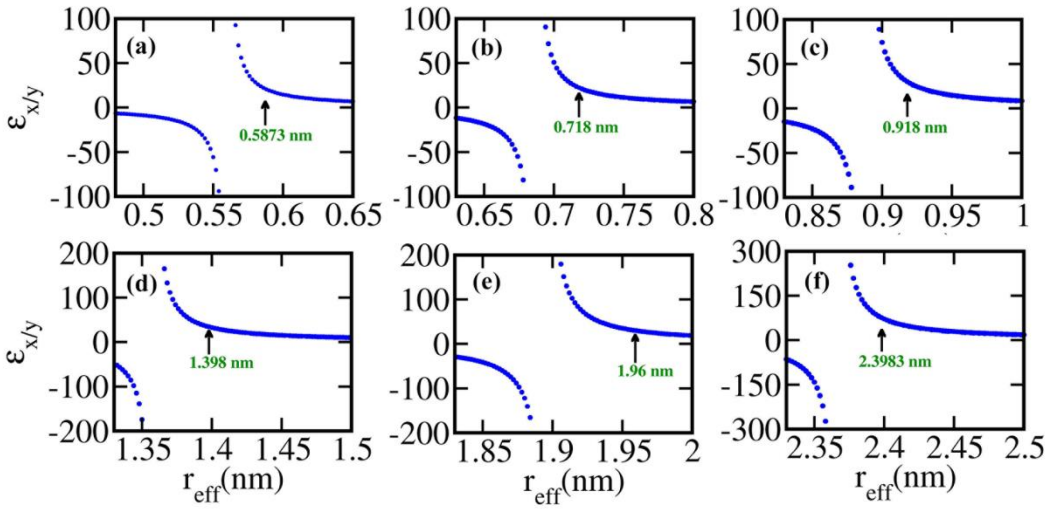

Figure S3. Sensitivity of the perpendicular static dielectric constant toward the effective/accessible volume of the cylindrical nanopores for (a) d=1.3 nm, (b) d=1.6 nm, (c) d=2.0 nm, (d) d=3.0 nm (e) d=4.0 nm, and (f) d=5.0 nm systems. The chosen values of the effective radii, estimated from the density profiles (Fig.2b in the main text), are marked by an annotated black arrow.

It is clear that the effective volume must be estimated accurately to avoid huge errors and unphysical values of $\varepsilon_{x/y}$. We tabulate the values of ε_z, $\varepsilon_{x/y}$, and the anisotropy parameter in **Table S3**, calculated using these estimated values of V_{eff} highlighted in **Figure S3**.

Table S3. The values of effective diameter, axial, and perpendicular static dielectric constants with the anisotropy parameter for six different sized CNT-water systems.

Nanotube diameter (nm)	Effective diameter (nm)	ε_z	$\varepsilon_{x/y}$	Anisotropy parameter (κ)
1.35	1.175	92.3 ± 0.45	20.3 ± 0.06	1.03
1.62	1.436	85.1 ± 0.31	22.2 ± 0.07	0.90
2.03	1.836	77.6 ± 0.42	30.1 ± 0.18	0.68
2.98	2.796	74.5 ± 0.16	34.2 ± 0.19	0.57
4.06	3.920	70.6 ± 0.15	43.0 ± 0.38	0.39
5.01	4.796	71.2 ± 0.31	71.4 ± 0.65	0.003

Interestingly, the difference between the actual diameter and the effective diameter is not fixed for all the systems studied. This indicates, in some systems the water molecules acquire a more compact configuration by increasing the intermolecular contacts and number of hydrogen bonds. This results in a decrease in the value of d_{eff}. The adaptation of either slightly inflated or compact configurations depend on the chosen number density of water

molecules inside the CNTs. We note that the number densities are not the same for all the confined systems. We obtain the number of water molecules from another set of equilibrium trajectories where the CNTs are attached to a water bath and seal them inside an infinite CNT along Z-axis (as described in **SI-2**).

4. Shell wise orientation distributions and anti-correlated coarse-grained dipole moments

In the main text, in **Figure 4** we have shown the shell wise orientation distribution of O-H bond vectors and the anti-correlated coarse grained time trajectories of the two vertically divided regions inside CNT for d=2.0 nm system. Here, in **Figure S4**, we provide similar graphs for other systems.

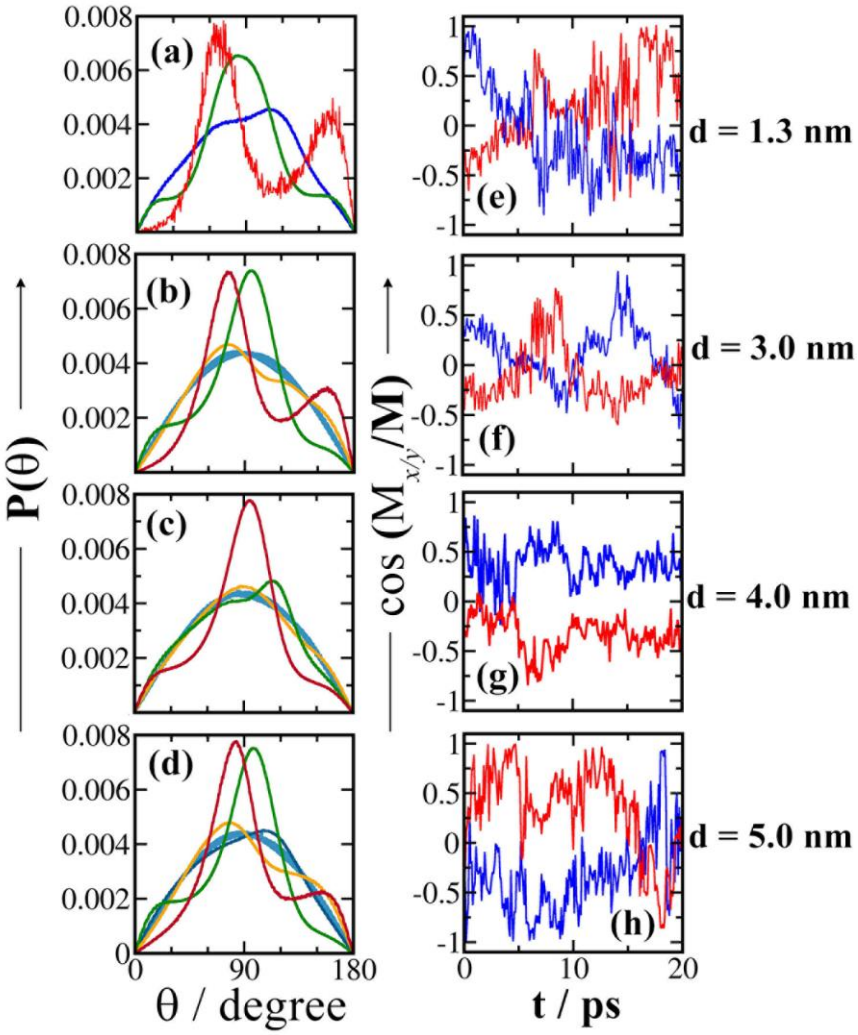

Figure S4. (a)-(d) Shell wise orientation distribution of water O-H bonds. The red traces represent the first layer closest to the surface. Green and orange traces represent second and third layers respectively. The blue traces represent all the central layers. (e)-(h) The anti-correlated time trajectories of region specific dipole moments associated with Pearson's correlation coefficients of -0.71, -0.74, -0.76, and -0.75 for d=1.3, 3.0, 4.0, and 5.0 nm CNT systems respectively.

5. Effective dielectric constant from spatially resolved dielectric profiles

Earlier studies by Renou *et al.*[8] and Schaaf *et al.*[9] reported spatial variation of axial $[\varepsilon_z(r)]$ and radial $[\varepsilon_z(r)]$ components of the static dielectric constant inside aqueous CNTs. For certain values of *r* the dielectric constant show a nearly 10 fold enhancement for smaller CNTs (**Figure S5**). Here, we show that the effective value of the dielectric constant can also be obtained from the previously reported dielectric profiles.

Before we proceed, we would like to raise a concern over the formalism. This is because the robustness of the scheme might depend on the coupling between different grids. According to the effective medium theory, we consider an inhomogeneous material of volume *V* enclosed by a surface *S*. The dielectric tensor, $\underline{\underline{\varepsilon}}(\mathbf{r})$, of such systems shows a spatial variation. Hence, an ensemble averaged and **r** independent quantity can be defined as

$$\varepsilon^{eff} = \lim_{V\to\infty} \frac{1}{V} \int_V d\mathbf{r}\, \varepsilon(\mathbf{r}) . \qquad \text{(SI.24)}$$

However, the validity of Eq. (SI.24) is subject to the following assumptions- (i) thermodynamic limit is valid, and (ii) the inhomogeneity is random. These two conditions are certainly not valid for confined systems where the radial profiles of density and dielectric permittivity shows a systematic pattern (**Figure S5**). Hence, Eq. (SI.24), that gets converted to Eq. (SI.26) for nanocylinders, is approximate. Nevertheless, because of the unavailability of exact formalism we use the same relation to extract some meaningful numbers from a previously reported dielectric profile.[8]

As an example, we consider the results reported by Renou *et al.* for CNT (20,20) with d=2.7 nm and L=10.0 nm. We extract the data (by using web digitizer software) from the paper and use that as the starting point.

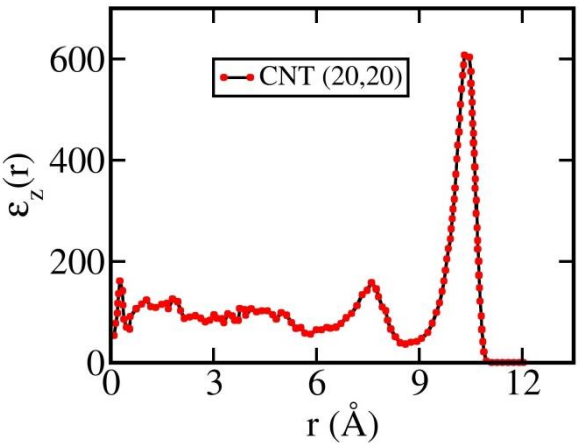

Figure S5. Radial profile of the z-component of the static dielectric constant obtained from the work of Renou *et al*. for CNT (20,20) [d=2.7 nm and L_z=10.0 nm]. This dielectric profile is used to calculate the effective dielectric constant along the z-direction.

We employ effective medium theory to obtain the effective values of ε_z from $\varepsilon_z(r)$ as shown in **Figure S5**. The expression for $\varepsilon_z(r)$ is as follows,

$$\varepsilon_z(r) = 1 + 4\pi\beta\left[\langle m_z(r)M_z\rangle_0 - \langle m_z(r)\rangle_0 \langle M_z\rangle_0\right] \quad \text{(SI.25)}$$

Therefore,

$$\varepsilon_z^{eff} = \frac{1}{V}\int_0^R dr\, \varepsilon_z(r)\, 2\pi r L \quad \text{(SI.26)}$$

We use Eq. (SI.25) in Eq. (SI.26) to obtain

$$\boldsymbol{\varepsilon}_z^{eff} = 1 + \frac{4\pi\beta}{V}\left[\langle \mathbf{M}_z^2\rangle_0 - \langle \mathbf{M}_z\rangle_0^{\,2}\right] \quad \text{(SI.27)}$$

Eq. (SI.27) is Eq. (4) in the main text. We perform the integral in Eq. (SI.26) numerically for the data shown in **Figure S5.** We obtain $\boldsymbol{\varepsilon}_z^{eff} = 92.4$ for d=2.7 nm and L=10.0 nm CNT. In the present work, we have found $\boldsymbol{\varepsilon}_z^{eff} = 74.5$ for d=2.98 nm and L=5.0 nm CNT. The values are close. Like ours, their data also shows an enhancement in $\boldsymbol{\varepsilon}_z^{eff}$. The slight difference could be because of the use of longer CNTs, a different LJ parameter combination [Werder *et al.* J. Phys. Chem. B., **2003**, 107 (6), p.1345] and a different water model (SPC/Ew) used.

References

1. Fröhlich, H. *Theory of dielectrics*. **1949**.
2. Jackson, J. D. *Classical electrodynamics*. John Wiley & Sons: **2012**.
3. Zhan, M. *Electromagnetic field theory: A problem solving approach*. Massachusetts Institute of Technology: **1979**.
4. Kubo, R. In *Linear response theory of irreversible processes*, Statistical Mechanics of Equilibrium and Non-equilibrium, **1965**; p 81.
5. Cornell, W. D.; Cieplak, P.; Bayly, C. I.; Gould, I. R.; Merz, K. M.; Ferguson, D. M.; Spellmeyer, D. C.; Fox, T.; Caldwell, J. W.; Kollman, P. A. A second generation force field for the simulation of proteins, nucleic acids, and organic molecules. *J. Am. Chem. Soc.* **1995**, *117*, 5179-5197.
6. Kayal, A.; Chandra, A. Exploring the structure and dynamics of nano-confined water molecules using molecular dynamics simulations. *Molecular Simulation* **2015**, *41*, 463-470.
7. Abraham, M. J.; Murtola, T.; Schulz, R.; Páll, S.; Smith, J. C.; Hess, B.; Lindahl, E. GROMACS: High performance molecular simulations through multi-level parallelism from laptops to supercomputers. *SoftwareX* **2015**, *1*, 19-25.
8. Renou, R.; Szymczyk, A.; Maurin, G.; Malfreyt, P.; Ghoufi, A. Superpermittivity of nanoconfined water. *J. Chem. Phys.* **2015**, *142*, 184706.
9. Schaaf, C.; Gekle, S. Spatially resolved dielectric constant of confined water and its connection to the non-local nature of bulk water. *J. Chem. Phys.* **2016**, *145*, 084901.